Elaboration of Novel NanoparticulateTiO_2-P25@n-TiO_2 Composite for Photocatalysis

Guy Didier Fanou[1,2], Benjamin Yao[2], Khley Cheng[1], Ovidiu Brinza[1], Mamadou Traoré[1], Andrei Kanaev[1] and Khay Chhor[1,*]

[1]*Laboratoire des Sciences des Procédés et des Matériaux (LSPM-CNRS) - Université Paris 13 Nord, Institut Galilée, France*

[2]*Laboratoire des Procédés de Synthèse, de l'Environnement et des Energies Nouvelles-LAPISEN; INP-HB; Cote d'Ivoire*

Abstract: A new mechanically stable TiO_2-P25@n-TiO_2 nanocoating was prepared after grafting of size-selected titanium-oxo-alkoxy particles on P25-TiO_2 nanoparticles surface and their immobilization on a glass substrate followed by a thermal treatment. The 5-nm oxo-TiO_2 particles were prepared in a sol-gel reactor with rapid reagents micromixing. The photocatalyst with 65% TiO_2-P25 loading shows the highest activity towards ethylene degradation in a continuous-flow fixed-bed reactor. This material has a higher activity compared to that prepared by a conventional sol-gel method with strongly polydispersed titanium-oxo-alkoxy nanoparticles and clusters. The reaction conditions were explicitly analyzed along the reactor as a function of the ethylene concentration in framework of a kinetic model, which shows interplay between zero and first order processes.

Keywords: TiO_2, Nanoparticles, Photocatalysis, Ethylene, Sol-gel.

1. INTRODUCTION

Gas solid heterogeneous photocatalytic reaction has received growing interest as a promising technology from researchers in recent years because of its wide potential applications for air purification. In these reactions, gaseous pollutants are oxidized over semiconductor particles illuminated with ultraviolet lamps or sunlight. The most common and low cost photocatalyst used in this technique is the commercial titanium dioxide TiO_2-P25 mainly due to its interesting electrochemical and photocatalytic properties that are largely applied in the field of photocatalysis for many applications such as water treatment, air purification and fuel cells [1-5]. For these applications, TiO_2-P25 particles are immobilized as films on different substrates such as fiber glass, glass rings, glass beads, glass wool, quartz sand, zeolites, silica or stainless steel [6-9]. However, films prepared with this photocatalyst suffer from the poor adhesion of deposit caused by the low chemical reactivity of TiO_2-P25 large particle size (~ 30 nm).This phenomenon limits their practical use due to the reduction of the purification system efficiency and the difficulties in their separation and recovery from treated effluent.

To improve mechanical properties of photocatalytic films, several researchers proposed a solution of preparing a composite by mixing TiO_2-P25 powder with TiO_2 particles obtained via sol-gel reaction. The prepared films by this method, called TiO_2-P25 modified powder sol-gel (PPMSG), after a heat treatment showed a good adherence and high photocatalytic activity [10, 11]. However, in these studies, no attention was given to the control of the particles size issued of the sol-gel reactions and their homogeneity. In the same time, these particles play a dominant role in the bond forming between TiO_2-P25 and substrate, capable influencing properties of the photocatalytic films.

Recently, a sol–gel reactor with turbulent mixing of reactive fluids [12, 13] permitted us to control the chemical reactions and stabilizing monodispersed titanium-oxo-alkoxy$Ti_xO_y(O^iPr)_z$ sols of a very small size. In particular, size-selected particles with diameters 2.0 nm, 3.2nm and 5.2nm were obtained [14].

In this article, the micromixing sol-gel method was used to fabricate new composite TiO_2-P25@n-TiO_2 photocatalyst, in which the TiO_2-P25 particles are bound to the substrate via titanium-oxo-alkoxy bonds. Because of their extremely high surface-to-volume ratio and chemical reactivity, the adherence of the films to substrates can be enhanced. Moreover, the photocatalytic activity of the prepared films is expected to be higher compared to those prepared via conventional deposition methods since the size-selected n-TiO_2 nanoparticles below 10 nm exhibit a very high photocatalytic activity [15]. We report on

*Address correspondence to this author at the Laboratoire des Sciences des Procédés et des Matériaux (LSPM-CNRS) - Université Paris 13 Nord, Institut Galilée, France; Tel: +33 1 49 40 34 12; Fax: +33 1 49 40 34 14;
E-mail: khay.chhor@lspm.cnrs.fr

E-ISSN: 2408-977X/16

structural properties of the P25@n-TiO_2 films and their photocatalytic kinetics and yield of ethylene photodegradation in a fixed-bed continuous-flow reactor.

2. EXPERIMENTAL SETUP

2.1. Chemicals

Titanium tetraisoproxide (TTIP) and propan-2-ol with respectively >98% and >99.5% purity were purchased from Acros Organics. TiO_2-P25 was used as supplied. Others reagents were of analytical grade and water was distilled.

2.2. Photocatalyst Preparation

The composite TiO_2-P25@ n-TiO_2 photocatalyst was prepared in three steps including (1) nanoparticles fabrication and mixing with TiO_2-P25 powder followed by (2) immobilization on glass bead support and (3) thermal treatment. The mixing of TiO_2 oxo-particles with TiO_2-P25 powder was achieved at the nucleation stage in which they are metastable and have a high reactivity. The sol nanoparticles are prepared in the sol–gel reactor using titanium tetraisopropoxide (TTIP) as a precursor. In the present experiments the standard operation conditions were conserved. Two stock solutions: 50 cm^3 of a TTIP/propan-2-ol solution and 50 cm^3 of a H_2O/propan-2-ol solution, was synchronously injected under nitrogen into the turbulent mixing zone (Re = 4500) of sol–gel reactor [13] where the oxo-TiO_2 nanoparticles were generated from hydrolysis-condensation reactions. The particle size can be tuned by adjusting the hydrolysis ratio $H = C_{H2O}/C_{TTIP}$, where C_{H2O} and C_{TTIP} are respectively water and titanium precursor concentrations. We have prepared colloids using hydrolysis ratio H = 2, which corresponds to one of stability domains of the sol–gel process and enables particles size of 5.2nm [14]. The suspended oxo-particles solution was subsequently transferred to a glove box LABstar MBraun where they were combined slowly with TiO_2-P25 powder under stirring. The mass ratio r of TiO_2-P25 to n-TiO_2 are 30, 40, 50, 65, 80 %. The immobilization of the colloidal nanoparticles on glass beads is achieved by dip-coating. The obtained films were finally dried at 80°C during 1hour followed by a heat treatment at 450°C during 4 hours.

2.3. Photocatalyst Characterization

The prepared samples were structurally characterised by X-ray diffraction XRD (INEL XRG 3000) using CuKα radiation with Nickel filter. The surface morphology of photocatalyst was examined by SEM JEOL JSM 64400F with acceleration voltage of 10 kV. Raman spectra were measured at 516 nm using micro-Raman high-resolution HR800 installation (HORIBA JobinYvon) with the spectral and spatial resolution respectively 0.25 cm^{-1} and 5 µm. The scattered light is collected by Peltier cooled CCD camera in a backscattering configuration.

The photocatalytic activity of the prepared samples was tested in a continuous-flow fixed-bed reactor on ethylene decomposition. A gas flow of pollutant (120 ppm) mixture with dry air and flow rate of 7.5 mL/min passes through a reactor tube of 6-mm diameter made of glass transparent in the UV-A spectral range [16, 17]. The glass beads coated photocatalyst samples were filled the reactor tube of 15 cm length. The tube is surrounded at a radial distance of 3 cm by six 8-W lamps emitting at 362 nm ($\Delta\lambda_{hwfm}$ = 22 nm). The reactor temperature 46 ± 2 °C was maintained during the experiments. Ethylene concentrations before (C_{in}) and after (C_{out}) the photocatalytic reactor were monitored by online gas chromatography (Varian 191 CP 3800) equipped with a capillary column (HP-PLOT/Q) and a flame ionization detector FID. Two injection loops of 250 µL and heated at 80 °C allow measurements of pollutant concentration in continuous mode. The reactor yield (or ethylene conversion) is calculated according to the formula: $\eta(\%) = (C_{in}-C_{out})/C_{in}\times100$. The column temperature and flow rate of the carrier gas (N_2) were respectively 50 °C and 5 mL/min.

3. RESULTS AND DISCUSSION

3.1. Thermal Analysis

Thermal studies were performed with TiO_2-P25@n-TiO_2 powder obtained with 40wt% of TiO_2-P25 loading. The results of differential thermal (DTA) and thermo gravimetric (TGA) analyses are shown in Figure **1**.

The results are closed to those obtained with a pure TiO_2 (not presented here). The quasi total mass loss was observed in the temperature range between 60 and 350 °C. This is attributed to departures of physically adsorbed solvent molecules, burning of the organic residues as well as the condensation of non-hydrolysed alkoxy groups [18, 19].

The crystallization of the anatase phase is associated with the exothermic peak at 379 °C on ATD curve which is markedly low compared to that of pure TiO_2 observed usually around 400 °C. According to Kumar *et al*. [20] crystallites nucleation and growth take

place at this point and the presence of TiO$_2$-P25 anatase in the composite can reduce the activation energy and promote the crystallisation process by decreasing the onset temperature.

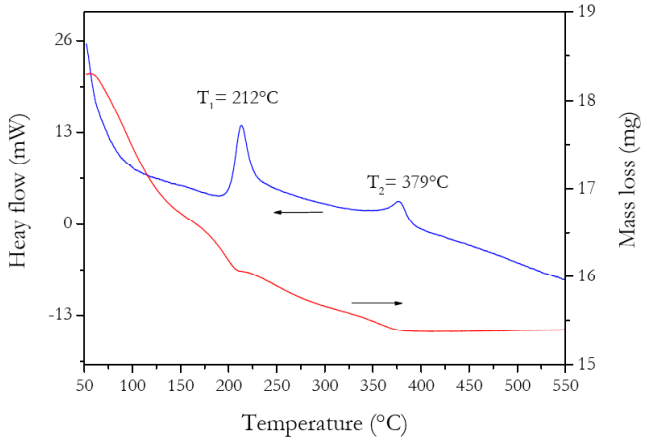

Figure 1: ATD-ATG curves of TiO2-P25@ n-TiO$_2$ composite. The oxo-TiO$_2$ preparation conditions are: C_{TTIP} = 0.15 M, H = 2, T = 20 °C, Re = 4500.

3.2. TEM, Raman and X Ray Diffraction Analyses

As we mentioned previously, the sol particles formed during the induction period of the sol-gel process (about 50 minutes by our experimental condition) are homogeneous of size close to 5.2 nm. Their general chemical composition is $TiO_{2(x+y)/2}(iOPr)_x(OH)_y$. They exhibit high reactivity and are capable forming strong covalent bonds with surface hydroxyls of TiO$_2$-P25 and substrate, as illustrated in Figure **2**.

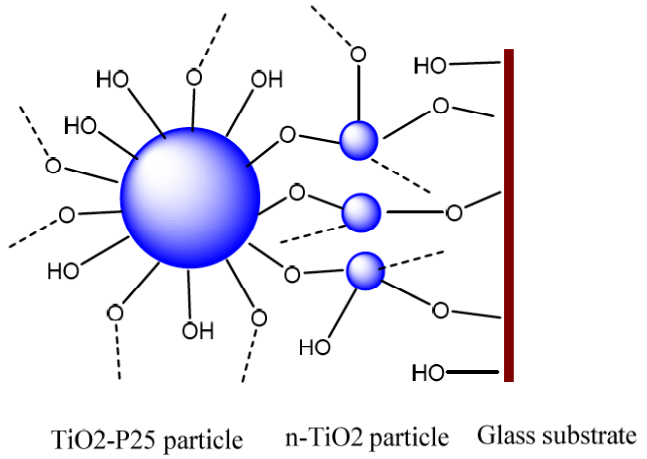

Figure 2: Diagram illustrating bond formation by n-TiO$_2$ particles allowing producing a composite film mechanically durable.

The TEM micrograph of TiO2-P25@n-TiO$_2$ composite shown in Figure **3** reveals that n-TiO$_2$ particles with diameter about 5 nm are attached to the surface of 30 nm TiO$_2$-P25 crystalline grains. Moreover this coverage sticks the grains together forming continuous structures. This result confirms the nanoparticulate nature of the coatings prepared using oxo-TiO$_2$ colloids; it is also in agreement with previous measurements carried out on the model mica substrate [16]. The chemical hydroxyls of the attached oxo-particles, not consumed for forming bounds between TiO$_2$-P25 grains, remain available to react with those of substrate resulting in a highly adherent nanocomposite film.

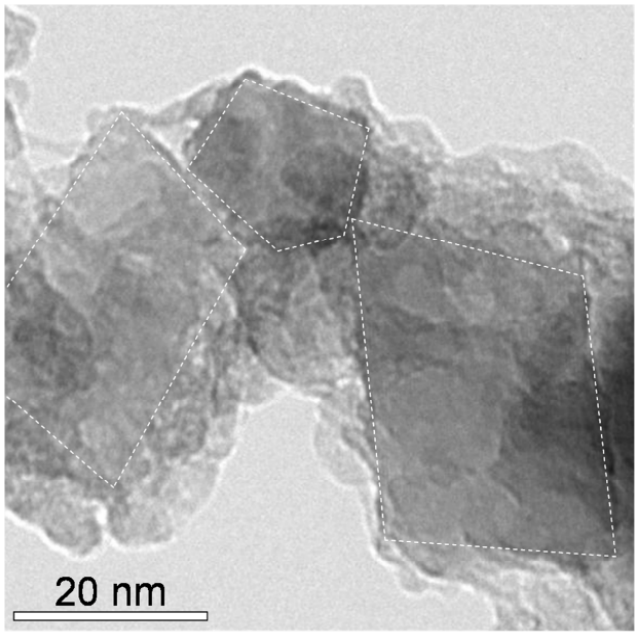

Figure 3: TEM micro graph of TiO$_2$-P25@ n-TiO$_2$ composite treated at 450°C and using r = 40% of TiO$_2$-P25 powder loading. TiO$_2$-P25 grains are shown by dashed line.

Because of a very small nanocoating mass of 10µg/cm^2, x-ray diffraction patterns of the thermally treated composite material were measured in the prepared powder-like samples. One of such patterns is shown in Figure **4**. The patterns of the coatings and powders are expected to be quite similar since, according to Martyanov and Klabunde [21], the substrate has little influence on the anatase phase crystallization, while can significantly increase the anatase-rutile transition temperature. Two principal RX diffraction peaks are observed at 25.07 and 27.25 ° respectively assigned to anatase (101) and rutile (110).Their intensity ratio (anatase/rutile) is much larger compared to the original pure TiO$_2$-P25 qualitatively indicating the presence of n-TiO$_2$ anatase phase in the composite.

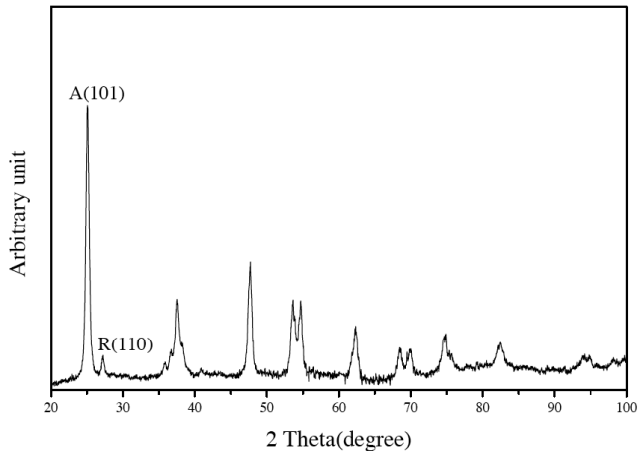

Figure 4: X-ray diffraction (XRD) diagrams of TiO_2-P25@n-TiO_2 composite prepared with 65% Degussa P25 loading and treated at 450 °C (4H). The colloid preparation conditions are C_{TTIP} = 0.15 M, H=2, T=20 °C, Re = 4500.

Raman spectrum of the composite powder is shown in Figure **5**. Several strong peaks are observed at 144, 400, 518 and 639 cm^{-1} for the anatase phase and are respectively attributed to vibrational modes E_g, B_{1g}, A_{1g}, E_g. The small amount rutile phase in TiO_2-P25@n-TiO_2 composite gives a weak rise of shoulders, the most intense of which appear at 443 and 610 cm^{-1} due to E_g and A_{1g} modes [22].

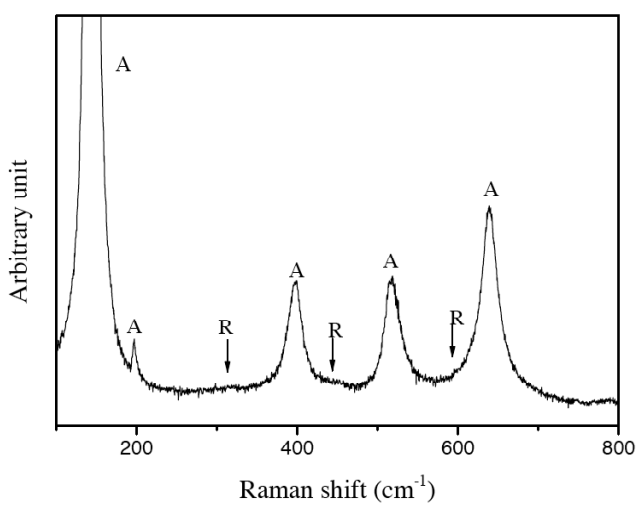

Figure 5: Raman spectra of TiO2-P25@n-TiO_2 composite prepared with H = 2, r = 65% treated at 450 °C. A and R denote the anatase and rutile phases respectively.

3.3. Photocatalytic Activity

The effect of TiO_2-P25 addition on the photocatalytic activity under UV radiation of TiO_2-P25@n-TiO_2 films was evaluated via photooxidation of ethylene in the presence of air. Figure **6** shows the pollutant conversion on the composite films prepared with r=30, 40, 50, 65, 80 wt%.

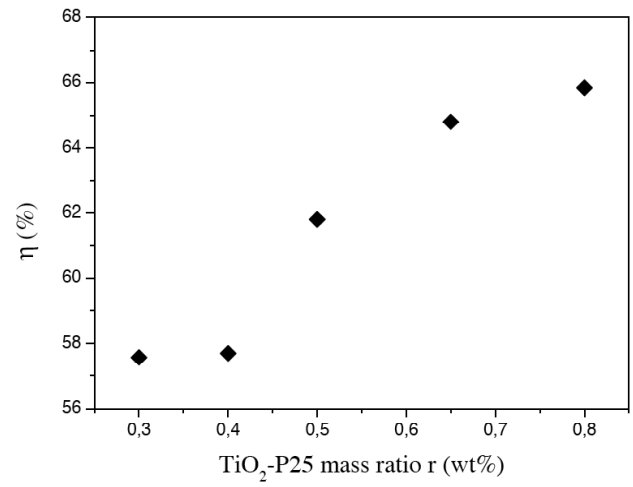

Figure 6: Ethylene conversion obtained by TiO_2-P25 @ n-TiO_2 films as a function of Degussa loading. The experimental conditions are C_{in}=120 ppm, pollutant residence time 5 s.

It can be noted that the ethylene conversion in the reactor increases by 10 % with the increase of TiO_2-P25 loading before stabilizing around 66 %. This enhancement in the composite activity may be explained by the total photocatalyst mass bound to the substrate and/or reduction of the immobilised particles size resulting in more optimal reaction conditions [23, 24]. Regarding the saturation of the photocatalytic activity, it can be explained by the common mass saturation effect as depicted by Herrmann [25].

Figure **7** shows the photocatalytic ethylene conversion by composite TiO_2-P25@n-TiO_2 prepared with 65% (correspondent to the saturation range in

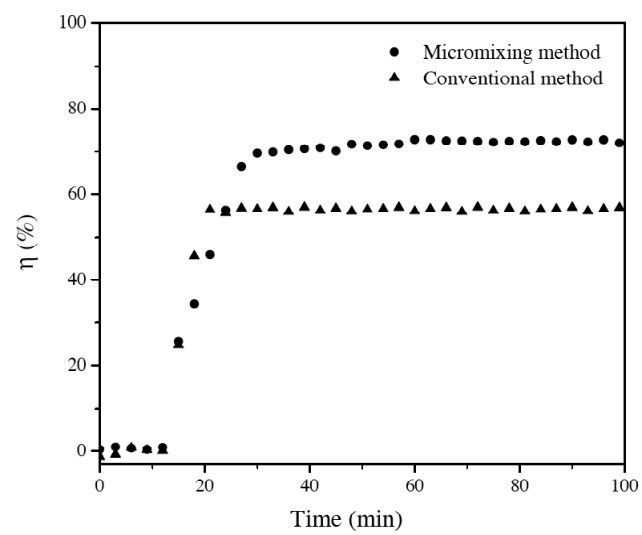

Figure 7: Ethylene photooxidation byTiO_2-P25 @ n-TiO_2 films prepared with r = 65% Degussa TiO_2 loading. The result with analogous composite obtained by conventional sol-gel method is given for comparison.

Figure **6**) of TiO$_2$-P25 loading and heat-treated at 450 °C for 4 hours using conventional sol-gel and micromixing methods. The enhancement of the conversion efficiency around 25% is recorded for the size-selected TiO$_2$-P25@n-TiO$_2$photocatalyst. In addition to a smaller size of the bound particles, this may be also related to a higher specific surface area 72 m^2/g of the size-selected composite compared to 57 m^2/g of that obtained by a conventional sol-gel method. We conclude that the homogeneous and reactive oxo-TiO$_2$ particles promote the bonds formation between TiO$_2$-P25 and substrate and enhance photocatalytic efficiency of the composite.

3.4. Reaction Order

The reaction order required a special consideration since defines the optimal conditions of the process. The fit of the experimental data with the phenomenological expression $dC/dt = kC^n$ proposed by Emeline *et al*. [26] adapted to a fix-bed continuous-flow reactor [17] is shown in Figure **8** and results in the reaction orders n=0.46±0.02. This indicates a significant presence of both zero and first order reaction kinetics.

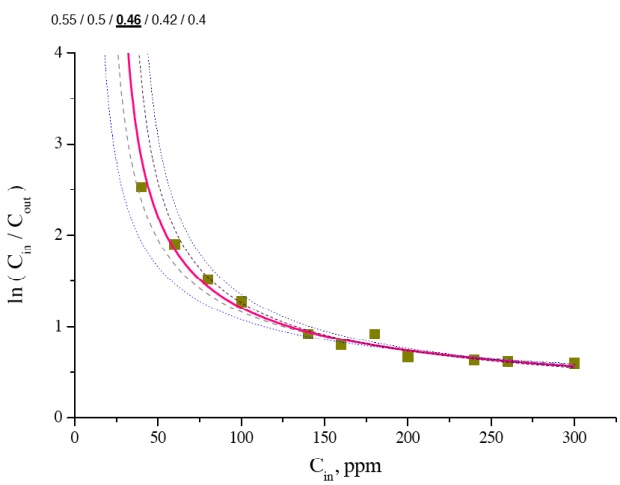

Figure 8: Fit of experimental data with the phenomenological expression of Emeline et al. [26] adapted to a continuous-flow fix-bed reactor [17].

More instructive in these conditions is to treat the experimental data with the exact solution of photocatalytic kinetics in the fix-bed continuous flow reactor. The solution can be found in our published article [17] and it is remind below.

The concentration dependence of the ethylene photooxidation rate can be explained by the Langmuir-Hinshelwood (L-H) model that takes into account chemical processes given below:

$$S + h\nu \rightarrow S^* \quad (1)$$

$$S^* \xrightarrow{\tau^{-1}} S \quad (2)$$

$$C \xleftrightarrow{k_d/k_a} C_{ads} \quad (3)$$

$$C + S^* \xrightarrow{k_r} P \quad (4)$$

where S, S*, C, C$_{ads}$ and p stand correspondingly for the ground-state and activated surface sites, gaseous and adsorbed pollutant concentrations and reaction products concentration and T, k$_a$, k$_d$ and k$_r$ are correspondingly excited state lifetime, adsorption, desorption and reaction constants. The solution of kinetic equation describing processes (1)-(4) in the continuous-flow fix-bed reactor is

$$a \cdot \ln\left(\frac{C_{in}}{C_{out}}\right) + \left(C_{in} - C_{out}\right) = bL \quad (5)$$

where $a = \left(k_d + k_r\right)/k_a$, $b = S_0 k_r / v$ from Eqs 1-4, S$_0$ is the total number density of available active surface sites and L is the reactor length. This expression can be respectively reduced to the pure 1st or 0 reaction orders when the first or second term in the left part of Eq. 5 dominate.The application of Eq. 5 to our experimental data is shown in Figure **9** by a solid line.

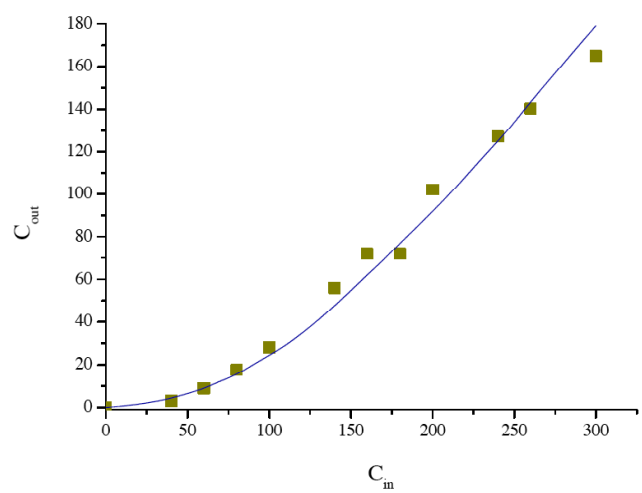

Figure 9: Fit of experimental data with Eq.5 for the mixed order process.

The agreement is quite good. Moreover, Eq. 5 permits clearly distinguishing between the two contributions of the 0 and 1st order reactions to the total process kinetics presented by the two terms.These contributions are shown in Figure **10**.

Evidently, the process kinetics follows the 1st order at low input ethylene concentrations. This regime

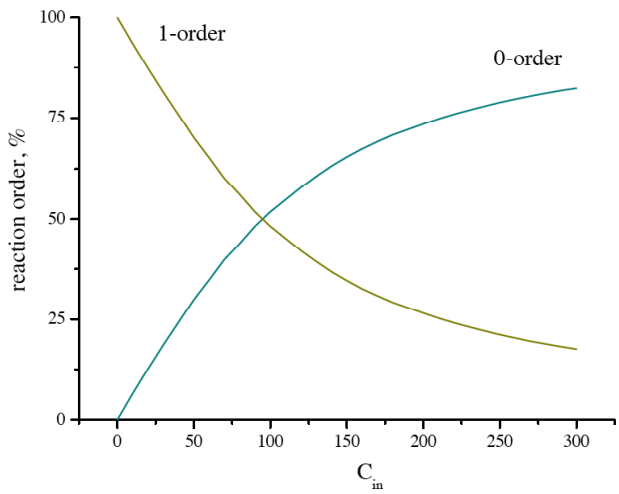

Figure 10: Contributions of zero and first order processes in the continuous flow reactor versus input concentration of ethylene.

corresponds to the non-saturated L-H adsorption of ethylene at the photocatalyst surface in the reactor at $0 \leq z \leq L$. With an increase of input concentration, the saturation first establishes in the reactor cross-section with a maximal concentration, which is C_{in} at the reactor input ($z = 0$). With the following increase of input concentration, the L-H adsorption saturation propagates along the reactor length z until $z = L$. When the saturation reaches $z = L$, the pure regime of the 0 order kinetics installs in the reactor. Accordingly, our experimental conditions 40 ppm < C_{in} < 300 ppm correspond to a regime of the saturation propagation along the reactor length $0 \leq z \leq L$ (Figure **10**). Resuming, the pure 0 and 1 order kinetics do not appear in our experimental conditions. However, experimental kinetics tends to almost pure 1 and 0 order respectively at ethylene concentration of below 50 ppm and above 300 ppm.

4. CONCLUSION

We report on the preparation of the mechanically stable TiO_2-P25@n-TiO_2 composite coating on a glass substrate after chemical colloid deposition of size-selected titanium oxo-alkoxy nanoparticles on TiO_2 P25 nanoparticles. The 5-nm oxo-TiO_2 nanoparticles were generated in a sol-gel reactor with rapid micromixing, grafted on TiO_2 P25 surface and immobilized on glass substrate at the beginning of the induction stage. The obtained films were dried at 80°C during 1 hour followed by a thermal treatment at 450°C during 4 hours. The photocatalytic test of ethylene degradation in a continuous-flow fixed bed reactor shows the maximum activity of the coating prepared with loading of 65 wt% TiO_2-P25, which may be explained by the retention of smaller immobilized particles resulting in more optimal reaction conditions. Kinetics studies are achieved using Langmuir-Hinshelwood model adapted to a fixed-bed continuous-flow reactor show a mixed reaction orders $n = 0.46 \pm 0.02$, which indicates a significant presence of both zero and first order reaction kinetics. An explicit analysis of this reaction regime shows that first and zero order processes dominate respectively at ethylene concentrations above and below 100 ppm. This analysis will be useful in optimisation of the photocatalytic process.

REFERENCES

[1] Fujishima A, Rao TN and. Tryk DA. Titanium Dioxide Photocatalysis, J Photochem Photobiol C: Photochem Rev 2000; 1: 1-21. http://dx.doi.org/10.1016/S1389-5567(00)00002-2

[2] Malato S, Blanco J, Vidal A and Richter C. Photocatalysis with solar energy at a pilot-plant scale: an overview, Appl Catal B Environ 2002; 37: 1-15. http://dx.doi.org/10.1016/S0926-3373(01)00315-0

[3] Wang TM, Wang HY, Xu P, Zhao XC, Liu YL and Chao S. The effect of properties of semiconductor oxide thin films on photocatalytic decomposition of dyeing waste water, Thin Solid Films 1998; 334: 103-108. http://dx.doi.org/10.1016/S0040-6090(98)01125-0

[4] Linesbigler AL, Lu G and Yates JT. Photocatalysis on TiO2 surfaces. Principle mechanisms and selected results, Chem Rev 1995; 95: 735-758. http://dx.doi.org/10.1021/cr00035a013

[5] Hurum DC, Agrios AG, Gray KA, Rajh T and Thurnauer MC. Explaining the Enhanced Photocatalytic Activity of Degussa P25 Mixed-Phase TiO2 Using EPR, J Phys Chem B 2003; 107: 4545-4549. http://dx.doi.org/10.1021/jp0273934

[6] Tompkins DT, Lawnicki BJ, Zeltner WA and Anderson MA. Evaluation of photocatalysis for gas-phase air cleaning -Part 1: Process; technical and sizing considerations, in: Geshwiler; M. (Ed.); Ashrae Transactions 2005; 111: 60.

[7] Fujishima A, Zhang X and Tryk DA. TiO2 photocatalysis and related surface phenomena, Surf Sci Rep 2008; 63: 515-582. http://dx.doi.org/10.1016/j.surfrep.2008.10.001

[8] Ohko Y, Hasimoto K and Fujishima A. Kinetics of photocatalytic reactions under extremely low intensity UV illumination on titanium dioxide thin films, J Phys Chem A 1997; 101: 8057-8062. http://dx.doi.org/10.1021/jp972002k

[9] Lasa HD, Serrano B and Salaices M. Photocatalytic reaction engineering, New York; USA: Springer Science; Business Media Inc., 2005.

[10] Chen Y and Dionysiou DD. Correlation of structural properties and film thickness to photocatalytic activity of thick TiO2 films coated on stainless steel, Appl Catal B: Environ 2006; 69: 24-33. http://dx.doi.org/10.1016/j.apcatb.2006.05.002

[11] Kenanakis G and Katsarakis N. Chemically grown TiO2 on glass with superior photocatalytic properties, J Environ Chem Eng 2014; 2: 1748-1755. http://dx.doi.org/10.1016/j.jece.2014.07.015

[12] Rivallin M, Benmami M. Kanaev A and Gaunand A. Sol-gel reactor with rapid micromixing: modelling and measurements of titanium oxide nano-particles growth, Chemical

Engineering Research & Design 2005; 83: 67-74. http://dx.doi.org/10.1205/cherd.03073

[13] Azouani R, Michau A, Hassouni K, Chhor K, Bocquet JF, Vignes JL *et al*. Elaboration of pure and doped TiO2 nanoparticles in sol-gel reactor with turbulent micromixing: application to nanocoatings and photocatalysis, Chemical Engineering Research & Design 2010; 88: 1123-1130. http://dx.doi.org/10.1016/j.cherd.2009.10.001

[14] Azouani R, Soloviev A, Benmami M, Chhor K, Bocquet JF and Kanaev A. Stability and growth of titanium-oxo-alcoxy TixOy(OiPr)z clusters, J Phys Chem C 2007; 111: 16243-16248. http://dx.doi.org/10.1021/jp073949h

[15] Benmami M, Chhor K and Kanaev A. High photocatalytic activity of monolayer nanocoatings prepared from non-crystalline titanium oxide sol nanoparticles, Chem Phys Lett 2006; 422: 552-557. http://dx.doi.org/10.1016/j.cplett.2006.03.001

[16] Benmami M, Chhor K and Kanaev A. Supported nanometric titanium oxide sols as a new efficient photocatalyst, J Phys Chem B 2005; 109: 19766- 19771. http://dx.doi.org/10.1021/jp051396+

[17] Tieng S, Kanaev A and Chhor K. New homogeneously doped Fe(III)-TiO2 photocatalyst for gaseous pollutant degradation, J Appl Catal A 2011; 399: 191-197. http://dx.doi.org/10.1016/j.apcata.2011.03.056

[18] Amores JMG, Escribano VS and Busca G. Anatase crystal growth and phase transformation to rutile in high-area TiO2, MoO3-TiO2 and other TiO2-supported oxide catalytic systems, J Mater Chem 1995; 5: 1245-1249. http://dx.doi.org/10.1039/JM9950501245

[19] Rodriguez-Talavera R, Vargas S, Arroyo-Murillo R, Montiel-Campos R and Haro-Poniatowski E. Modification of the phase transition temperatures in titania doped with various cations, J Mater Res 1997; 12: 439-443 http://dx.doi.org/10.1557/JMR.1997.0065

[20] Kumar KNP, Keizer K, Burggraaf AJ, Okubo T, Nagamoto H and Morooka S. Densification of nanostructured titania assisted by a phase transformation, Nature 1992; 358: 48-51. http://dx.doi.org/10.1038/358048a0

[21] Martyanov IN and Klabundev. Comparative study of TiO2 particles in powder form and as a thin nanostructured film on quartz, J Catal 2004; 225: 408-416. http://dx.doi.org/10.1016/j.jcat.2004.04.019

[22] Balachandran U and Eror NG. Raman spectrum of titanium dioxide, J Solid State Chem 1982; 42: 276-282. http://dx.doi.org/10.1016/0022-4596(82)90006-8

[23] Chen Y and Dionysiou DD. TiO2 photocatalytic films on stainless steel: The role of Degussa P-25 in modified sol-gel methods, Appl Catal B: Environ 2006; 62: 255-264. http://dx.doi.org/10.1016/j.apcatb.2005.07.017

[24] Bouslama M, Amamra MC, Jia Z, Amar MB, Brinza O, Chhor K *et al*., New nanoparticulate TiO2-Al2O3 photocatalytic media: Effect of particle size and polymorphism on photocatalytic activity, ASC Catal 2012; 2: 1884-1892.

[25] Herrmann JM. Heterogeneous photocatalysis: fundamentals and applications to the removal of various types of aqueous pollutants, Catal Today 1999; 53: 115-129. http://dx.doi.org/10.1016/S0920-5861(99)00107-8

[26] Emeline AV, Ryabchuk V and Serpone N. Factors affecting the efficiency of a photocatalyzed process in aqueous metal-oxide dispersions: Prospect of distinguishing between two kinetic models, J Photochem Photobiol A 2000; 133: 89-97. http://dx.doi.org/10.1016/S1010-6030(00)00225-2

Received on 20-09-2016 Accepted on 06-10-2016 Published on 10-10-2016

http://dx.doi.org/10.15379/2408-977X.2016.03.01.04